Electronic Supplementary Material (ESI) for Journal of Materials Chemistry A.
This journal is © The Royal Society of Chemistry 2023

Boosting trace SO_2 adsorption and separation performance by the modulation of the SBU metal component of iron-based bimetal MOF

Jinze Yao,[a†] Zhiwei Zhao,[b†] Liang Yu,[a] Jiajin Huang,[a] Shigen Shen,[a] Siyao Zhao,[a] Ying Wu, [c*]Xiangyang Tian,[a] Jun Wang,[b*]Qibin Xia[a*]

[a] *School of Chemistry and Chemical Engineering, South China University of Technology, Guangzhou 510640, P. R. China*

[b] *School of Chemistry and Chemical Engineering, Nanchang University, Nanchang, Jiangxi 330031, P.R China*

[c] *School of Chemical Engineering and Light Industry, Guangdong University of Technology, Guangzhou, Guangdong 510006, P. R. China.*

† Jinze Yao and Zhiwei Zhao contributed equally to this work

Materials

The Zinc nitrate hexahydrate [$Zn(NO_3)_2 \cdot 6H_2O$, 99.0%] were obtained from Aladdin Reagent (Shanghai) Co., LTD. The iron nitrate nonahydrate [$Fe(NO_3)_3 \cdot 9H_2O$, 98.5%], cobalt nitrate hexahydrate [$Co(NO_3)_2 \cdot 6H_2O$, 98.5%], nickel nitrate hexahydrate [$Ni(NO_3)_2 \cdot 6H_2O$, 98.5%] and manganese tetrahydrate nitrate [$Mn(NO_3)_2 \cdot 4H_2O$, 98.0%] were purchased from the Tianjin Damao Chemicals Co., Ltd. The organic ligand 3,3′,5,5′-azobenzenetetracarboxylic acid (H_4ABTC, 99.0%) was obtained from Shanghai Chemsoon Chemical Co., Ltd. Anhydrous sodium acetate (CH_3COONa, 99.0%), ethanol (EtOH, 99.7%), dichloromethane (CH_2Cl_2,

* Corresponding authors at:
[1] School of Chemistry and Chemical Engineering, South China University of Technology, Guangzhou 510640, PR China
[2] School of Chemistry and Chemical Engineering, Nanchang University, Nanchang, Jiangxi 330031, P.R China
[3] School of Chemical Engineering and Light Industry, Guangdong University of Technology, Guangzhou, Guangdong 510006, P. R. China.
E-mail: qbxia@scut.edu.cn (Q. B. Xia)[1], jwang7@ncu.edu.cn (J. Wang), yingwu@gdut.edu.cn (Y. Wu)[3]

99.5%), N, N-dimethylformamide (DMF, 99.5%), methanol (MeOH, 99.5%), and glacial acetic acid (CH_3COOH, 99.5%) were obtained from the Tianjin Damao Chemicals Co., Ltd. Ultrapure. Ultrahigh-purity-grade (>99.99%) N_2 and high-purity-grade (>99.95%) SO_2, CO_2 and CH_4 gases were used during the adsorption experiments.

Synthesis of preformed metal clusters

The $Fe_3(\mu_3\text{-}O)(CH_3COO)_6$ clusters were synthesized as literature reported with modifications[1-3]. Generally, dissolve iron nitrate nonahydrate (4.04 g, 0.01 mol) and sodium acetate (12.72 g, 0.155 mol) in 25 ml of deionized water, respectively. After that, the CH_3COONa solution was dropwise added into the iron (III) nitrate solution under stirring. Brown precipitate could be obtained after stirring the mixed solution overnight. The product was filtrated and washed with EtOH, and then, dried at 343 K for 6 h under vacuum. For $Fe_2M(\mu_3\text{-}O)(CH_3COO)_6$ (M = Ni, Co, Zn, Mn), the preparation process was the same as $Fe_3(\mu_3\text{-}O)(CH_3COO)_6$ except that the M(II) (M = Co, Ni, Zn, Mn) nitrate (0.05 mol) was mixed with the iron(III) nitrate before dissolution.

Synthesis of PCN-250 series materials

PCN-250 and bimetal PCN-250(Fe_2M, M = Ni, Co, Zn, Mn) were synthesized as previously reported with minor modifications[3]. In a typical procedure, $Fe_3(\mu_3\text{-}O)(CH_3COO)_6$ clusters (15 mg), H_4ABTC (10 mg), DMF (2 mL), and CH_3COOH (1.4 mL) were added into a 23 ml Pyrex vial. The mixed solution was then heated in an oven for 12 h at 413 K. After slowly cooled to room temperature, the obtained brown crystal was filtrated and washed with DMF. The synthesis of bimetal PCN-250 (Fe_2M, M = Co, Ni, Zn, Mn) was the same as the original PCN-250 material, except that corresponding $Fe_2M(\mu_3\text{-}O)(CH_3COO)_6$ (Fe_2M, M = Ni, Co, Zn,

Mn) clusters were selected. Moreover, in the preparation of PCN-250(Fe_2Mn), the amount of CH_3COOH added was reduced to 1.1 mL.

Large-scale synthesis of PCN-250 series MOF

PCN-250(Fe_2M), M=Fe, Co, Ni, Mn, Zn were synthesized according to the reported literature, with some adjustments[1]. $Fe_3(\mu_3\text{-}O)(CH_3COO)_6$ clusters (1 g), H_4ABTC (1 g), DMF (200 mL), and CH_3COOH (140 mL) were added into a 500 mL Pyrex vial. The mixed solution was then heated in an oven for 12 h at 413 K. After slowly cooled to room temperature, the obtained brown crystal was filtrated and washed with DMF. The synthesis of bimetal PCN-250 (Fe_2M, M = Co, Ni, Zn, Mn) was the same as the original PCN-250 material, except that corresponding $Fe_2M(\mu_3\text{-}O)(CH_3COO)_6$ (Fe_2M, M = Ni, Co, Zn, Mn) clusters were selected. Moreover, in the preparation of PCN-250(Fe_2Mn) and PCN-250(Fe_2Zn), the amount of CH_3COOH added was reduced to 120 mL and 100 mL, respectively.

Characterization Methods

Powder X-ray diffraction (XRD) patterns were acquired on a Bruker D8 Advance X-ray diffractometer at 40 kV and 40 mA with a scan speed of 0.02°/s in the 2θ range of 5-50° using Cu-Kα radiation. Thermogravimetric analysis (TGA) was conducted under N_2 atmosphere at a heating rate of 10 ℃/min from room temperature to 600 ℃ using a TGA-55 instrument. Scanning electron microscope (SEM) images were obtained on a TESCAN MIRA4 instrument. N_2 adsorption and desorption isotherms were measured at 77 K on ASAP 2460 Analyzer (Micromeritics) equipped with commercial software for calculation and analysis. The surface area was estimated by Brunauer-Emmett-Teller (BET) equation and the pore size distribution

was calculated based on the density functional theory (DFT) method.

Simulation methods

To reveal the intrinsic mechanism for the superior separation behavior, computational modeling was conducted to investigate SO_2 and CO_2 adsorption in PCN-250 series materials. Adsorption density simulations were performed in the Sorption module, in which one molecule of each adsorbate was loaded (fixed loading) in 2 × 2 × 2 unit cell of the framework by means of the Metropolis Monte Carlo (MC) method at 298 K. This MC method sample an ensemble by generating a chain of configurations with the ensemble density. Exchange, conformers, rotate, translate and regrow trials of the adsorbate with probability of 0.39, 0.20, 0.20, 0.20, 0.02 were considered in each MC step. QEq method was used to calculate the partial charges of the adsorbate and adsorbent, in order to describe the electrostatic interactions with the Ewald summation method under an accuracy of 1×10^{-4} kcal/mol. Van der Waals interactions between adsorbate and adsorbent were described by the universal force field, where the interactions were truncated at 15.5 Å. During the calculations, 1×10^{5} steps were used for equilibration, and 1×10^{6} steps were used for production. The charge density difference between the guest molecules and framework was derived from density functional theory (DFT) calculations taking the generalized gradient approximation (GGA) with a Perdew-Burke-Ernzerh (PBE) as the exchange-correlation functional with the CASTEP package. The guest molecules were isolated from the framework for the charge density difference calculation. The k-point was 3x3x3.

Calculation of equilibrium selectivity

The SO_2, CO_2, CH_4 and N_2 adsorption isotherms were fitted by the dual site Langmuir-Freundlich (DSLF) model. The DSLF equation can be expressed as the follows:

$$q = q_1 \frac{b_1 p^{c_1}}{1 + b_1 p^{c_1}} + q_2 \frac{b_2 p^{c_2}}{1 + b_2 p^{c_2}} \qquad (1)$$

where q (mmol/g) is the equilibrium adsorbed amount for an adsorbent, q_1 and q_2 (mmol/g) are the saturated adsorption capacities of site 1 and site 2, b_1 and b_2 are the affinity coefficients for sites 1 and 2, p (kPa) is the equilibrium pressure of the bulk gas, and c_1 and c_2 are the deviations from an ideal homogeneous surface. Both the pure component isotherms are well fitted by the model and the R^2 values are larger than 0.995 (see Table S1). The adsorption selectivities S were determined by IAST calculations. IAST equation is given below:

$$S = \frac{q_1/q_2}{p_1/p_2} \qquad (2)$$

where q_1 and q_2 are the adsorbed amounts of the adsorbed phase for component 1 and 2, respectively and p_1 and p_2 refer to the pressures in the gas phase for component 1 and 2, respectively.

Calculation of isosteric heat of adsorption. To evaluate the adsorption interactions between gas molecules and the MOF framework, as an important thermodynamic parameter, the isosteric heat of adsorption (Q_{st}) was calculated by fitting SO_2, CO_2, CH_4 and N_2 sorption isotherms measured at 288, 298, and 308 K using the Virial equation.

$$lnP = lnN + \sum_{i=0}^{m} a_i N^i + \sum_{i=0}^{n} b_i N^i \quad (1)$$

where P is the pressure (bar); N is the amount adsorbed (mmol/g); T is the temperature (K); a_i and b_i are Virial coefficients; m and n determine the number of coefficients required to accurately describe the isotherms. Then, the values of the Virial coefficients a_0 to a_m are employed to obtain the isosteric heat of adsorption from the following equation as a function of SO_2, CO_2, CH_4 and N_2 sorption amounts, respectively.

$$Q_{st} = -R\sum_{i=0}^{m} a_i N^i \quad (2)$$

where R is the gas constant [8.314 J/(K·mol)].

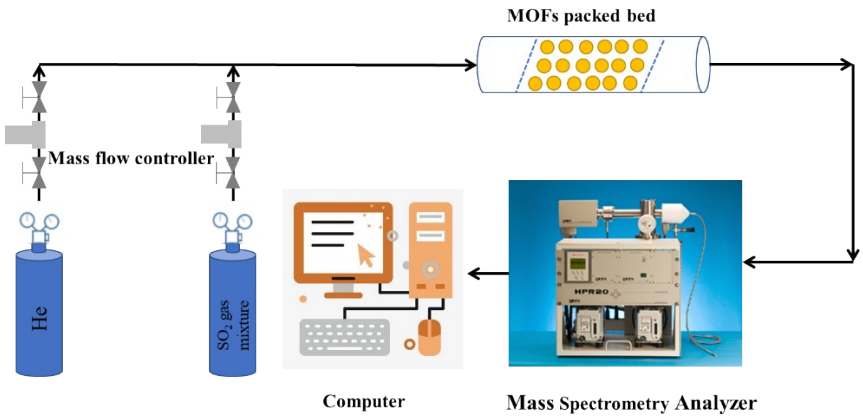

Scheme. S1. Schematic illustration of the homemade set-up used for the breakthrough experiments.

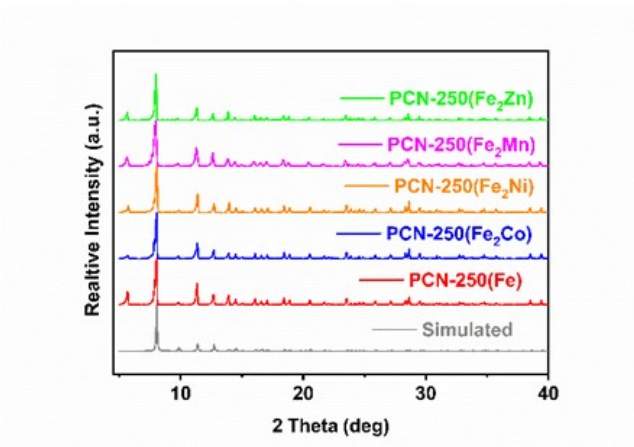

Fig. S1 PXRD curves of PCN-250 series materials

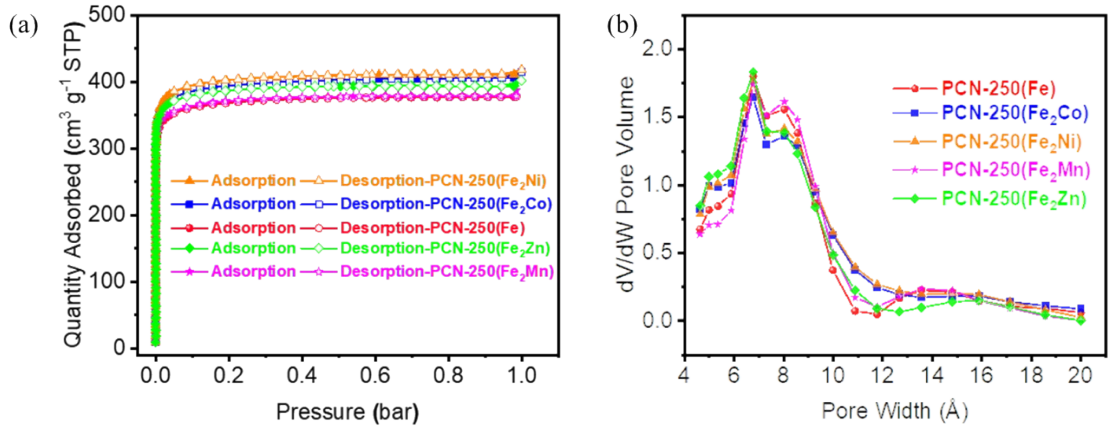

Fig. S2 (a) N_2 adsorption-desorption isotherms at 77 K (b) pore size distribution of PCN-250 series materials

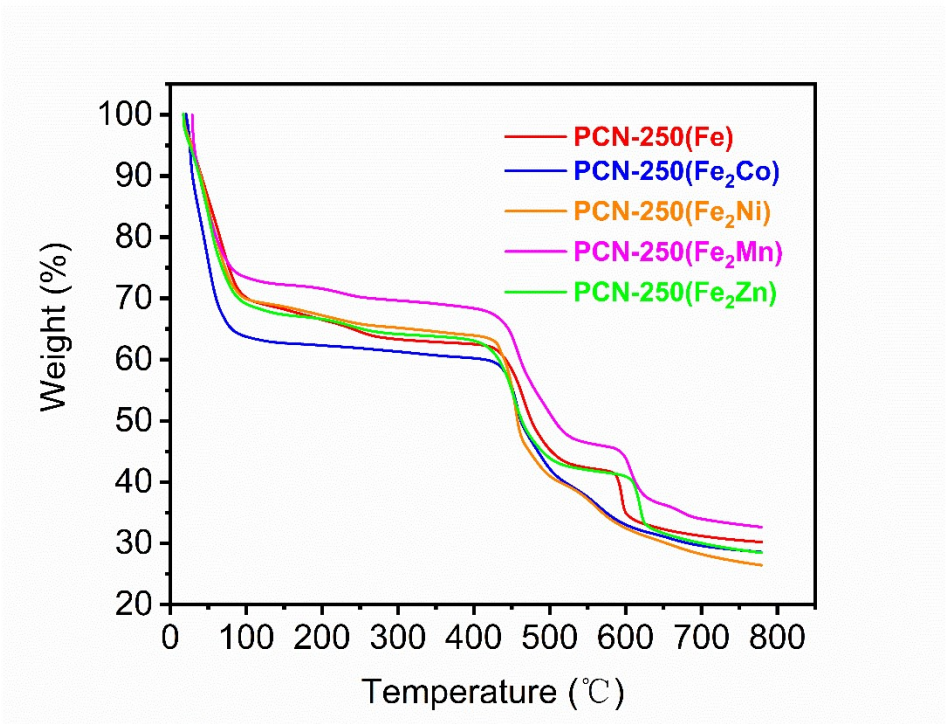

Fig. S3 The TGA curve of PCN-250 series materials.

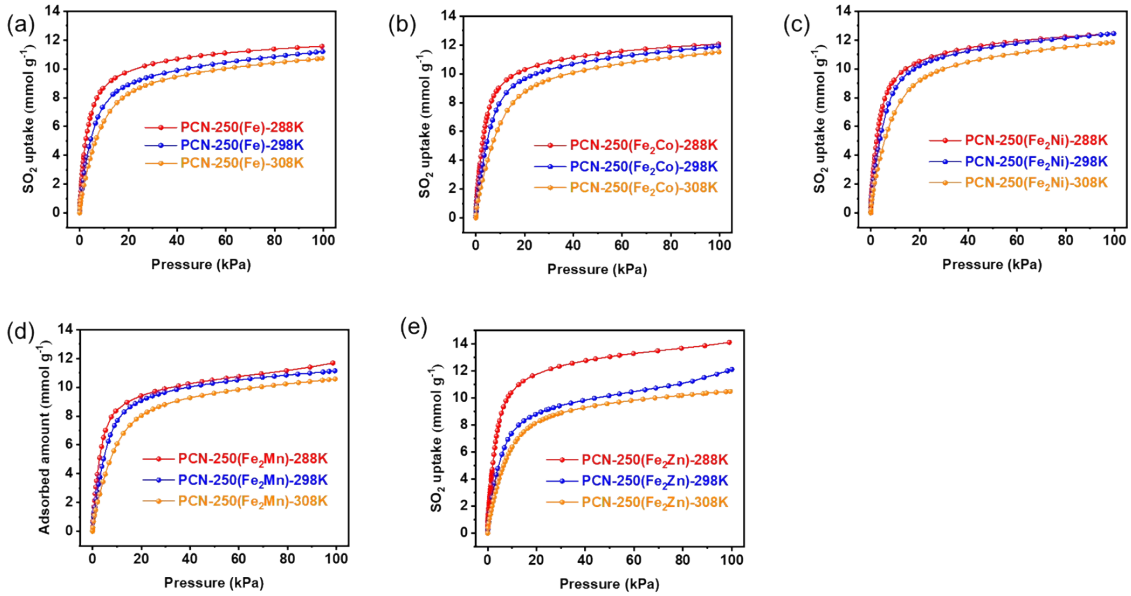

Fig. S4 The SO_2 adsorption isotherms of PCN-250 series materials at 288, 298 and 308 K.

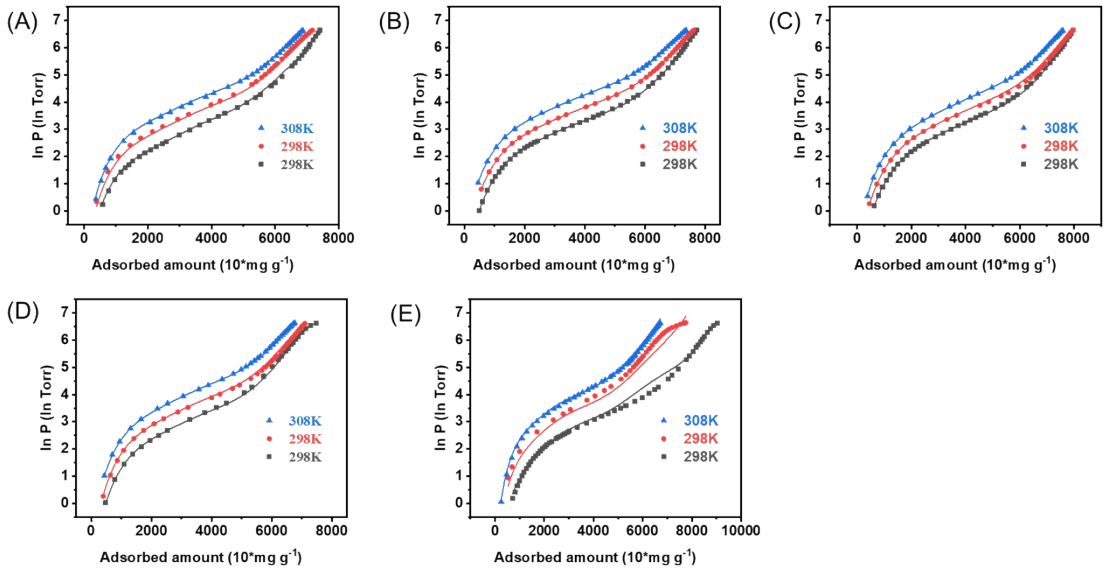

Fig. S5 Virial fitting (lines) of SO_2 adsorption isotherms (points) of PCN-250 series materials measured at 288 K (blue), 298 K (red), and 308 K (black)

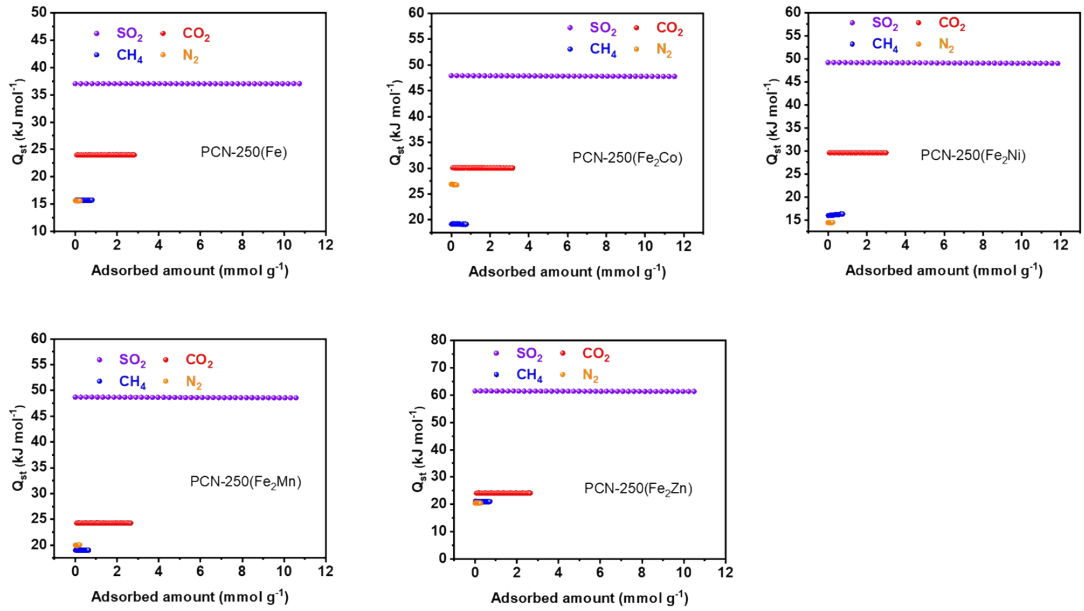

Fig. S6 The isosteric heat of SO_2, CO_2, CH_4 and N_2 of five materials.

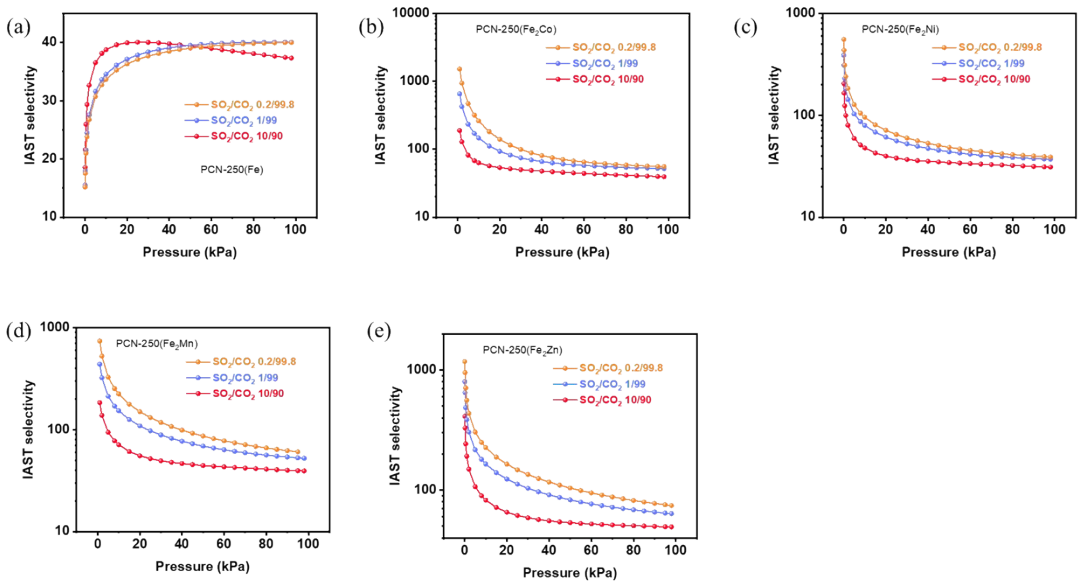

Fig. S7 The ideal adsorption solution theory (IAST) selectivity of SO_2/CO_2 (10:90, 1:99 and 0.2/99.8, v:v) mixtures of five PCN-250 materials.

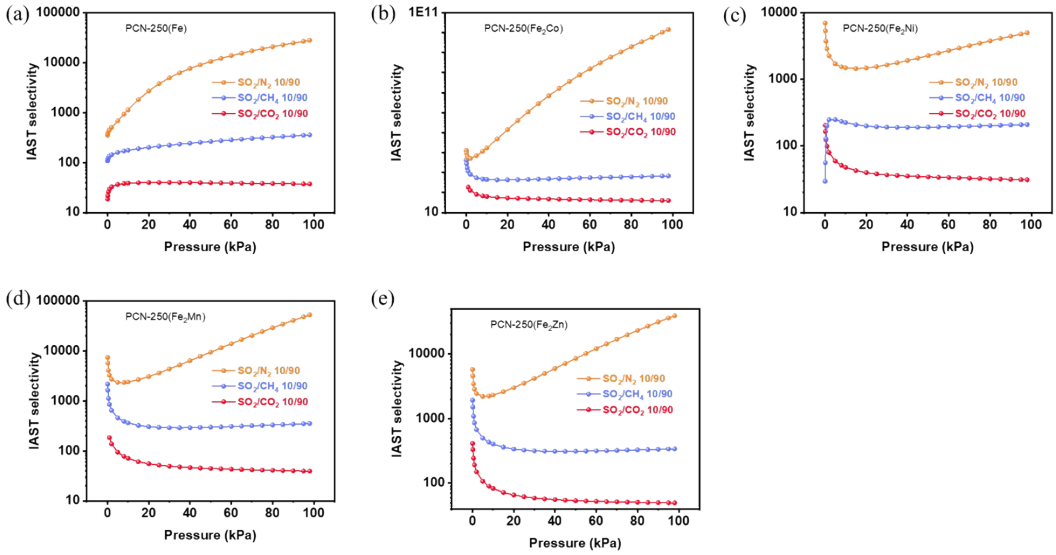

Fig. S8 The ideal adsorption solution theory (IAST) selectivity of SO_2/CO_2 (10:90, v:v), SO_2/CH_4 (10:90, v:v) and SO_2/N_2 (10:90, v:v) mixtures of five PCN-250 materials.

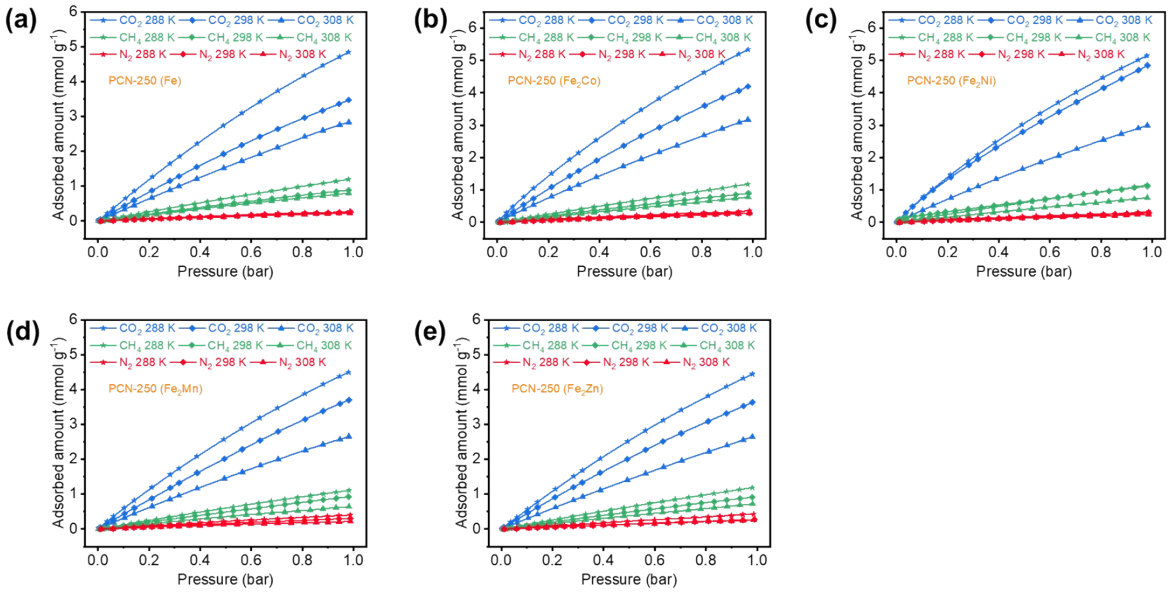

Fig. S9 The CO_2, CH_4 and N_2 adsorption isotherms of PCN-250 series materials at 288, 298 and 308 K.

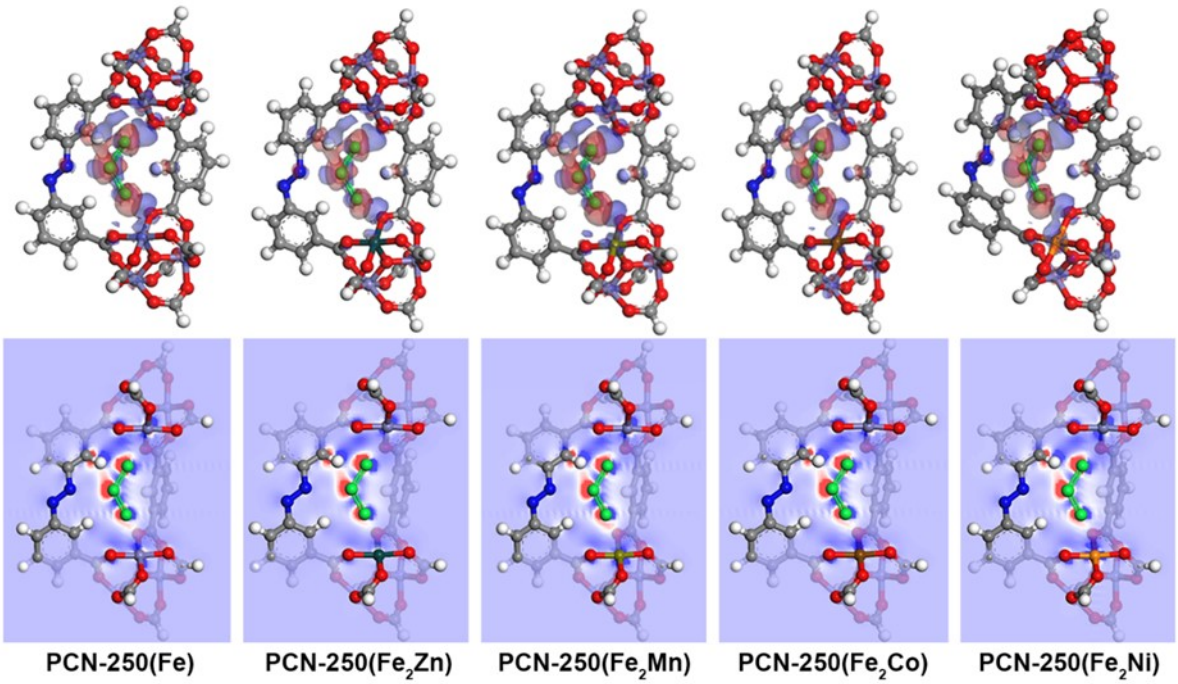

Fig. S10 Charge density difference of SO_2-adsorbed PCN-250 series materials. The electron density increases in the red region and decreases in the blue region.

Table S1. Pore textural parameters of PCN-250 series materials.

Material	BET Surface areas (m^2/g)	pore volume (cm^3/g)
PCN-250 (Fe)	1495	0.48
PCN-250 (Fe_2Co)	1583	0.51
PCN-250 (Fe_2Ni)	1621	0.52
PCN-250 (Fe_2Mn)	1483	0.47
PCN-250 (Fe_2Zn)	1560	0.50

Table S2. Adsorption capacities of SO_2 and CO_2 on PCN-250 series materials and their capacity difference at 298 K and 100 kPa.

	PCN-250 (Fe)	**PCN-250 (Fe_2Co)**	**PCN-250 (Fe_2Ni)**	**PCN-250 (Fe_2Mn)**	**PCN-250 (Fe_2Zn)**
$n(SO_2)$ (mmol/g)	11.21	11.92	12.44	11.14	12.11
$n(CO_2)$(mmol/g)	3.47	4.20	4.84	3.70	3.63
$n(SO_2)$-$n(CO_2)$ (mmol/g)	7.74	7.72	7.6	7.44	**8.48**

Table S3. C_2H_6 and C_2H_4 fitting parameters of the Dual Site Langmuir-Freundlich model at 298 K of PCN-250 series materials.

		q_1	b_1	c_1	q_2	b_2	c_2	R^2
PCN-250 (Fe)	SO_2	238	0.00001153	1.442	10.06	0.1935	1.124	0.9988
	CO_2	5.77	0.0048	0.8276	9.339	0.001951	1.131	0.9999
	CH_4	5.402	0.001728	1.03	0.0291	0.000301	0.8626	0.9999
	N_2	0.7402	0.002413	1.131	2.741	0.0003515	0.7487	0.9999
PCN-250 (Fe_2Co)	SO_2	5.899	0.2226	1.638	11.19	0.1177	0.4402	0.9999
	CO_2	10.97	0.001405	1.145	5.511	0.007013	0.9922	0.9999
	CH_4	5.545	0.001019	1.101	0.2866	0.01111	0.9235	0.9999
	N_2	0.5148	0.002433	1.168	0.2398	0.005441	1.087	0.9999
PCN-250 (Fe_2Ni)	SO_2	9.655	0.2142	0.607	4.331	0.03105	2.173	0.9999
	CO_2	14.63	0.0001733	1.453	6.833	0.01357	0.8889	0.9999
	CH_4	2.584	0.0349	0.2813	7.506	0.0004891	1.203	0.9999
	N_2	2.015	0.0003257	1.227	1.302	0.002062	0.8485	0.9999
PCN-250 (Fe_2Mn)	SO_2	8.979	0.2226	0.5976	4.097	0.03174	2.203	0.9999
	CO_2	6.405	0.002952	0.95	12.39	0.002101	1.033	0.9999
	CH_4	6.09	0.0009101	1.099	0.3756	0.01044	0.9128	0.9999
	N_2	0.9807	0.001455	1.036	0.8739	0.00146	1.035	0.9998
PCN-250 (Fe_2Zn)	SO_2	10.4	0.2436	0.6572	3.692	0.02347	2.391	0.9999
	CO_2	8.726	0.001096	1.254	5.789	0.006193	0.8651	0.9999
	CH_4	7.772	0.0004577	1.16	0.639	0.009016	0.9333	0.9999
	N_2	2.195	0.00139	1.032	0.1141	0.0001603	0.8728	0.9996

Table S4. Fitting parameters of the virial equation and the correlation coefficients.

		a_0	a_1	a_2	a_3	a_4	b_0	b_1	R^2
PCN-250 (Fe)	SO_2	-4451.88	-0.0789	9.15E-05	-2.35E-07	1.78E-10	8.35396	0.00252	0.9990
	CO_2	-2887.59	-0.26379	5.97E-04	1.99E-06	-4.98E-09	8.71931	0.00146	0.9998
	CH_4	-1890.78	-6.2116	0.34315	-0.00684	9.66E-05	7.96669	0.00753	0.9991
	N_2	-2887.59	-0.26379	5.97E-04	1.99E-06	-4.98E-09	8.71931	0.00146	0.9998
PCN-250 (Fe_2Co)	SO_2	-5763.59	1.53815	-2.74E-04	-1.96E-07	1.25E-10	13.15723	-0.00396	0.9999
	CO_2	-3617.89	1.84872	-0.00138	-5.97E-07	1.18E-09	10.99595	-0.00656	0.9999
	CH_4	-2305.75	3.4099	1.08614	-0.04257	7.63E-04	9.68059	-0.07926	0.9989
	N_2	-3234.45	52.78926	7.15309	-0.58973	0.01987	13.95964	-0.48297	0.9957
PCN-250 (Fe_2Ni)	SO_2	-5914.76	1.91113	-4.53E-04	-4.66E-08	4.64E-11	13.43236	-0.00508	0.9990
	CO_2	-3561.60	0.09322	0.0016	-7.10E-06	1.32E-08	10.62477	-5.36E-04	0.9940
	CH_4	-1920.30	-59.4937	3.35425	-0.09201	0.00139	8.41475	0.01581	0.9079
	N_2	-1734.35	-45.6261	6.73451	-0.45254	0.01619	8.60903	-0.04436	0.9991
PCN-250 (Fe_2Mn)	SO_2	-5860.40	1.71088	-5.34E-04	-8.05E-08	1.05E-10	13.27391	-0.00371	0.9988
	CO_2	-2921.08	0.67034	-0.00106	-1.35E-06	4.34E-09	8.87314	-0.00235	0.9998
	CH_4	-2285.92	-5.6696	0.87018	-0.04114	8.37E-04	9.56874	-0.03833	0.9980
	N_2	-2404.62	-20.2806	4.17029	-0.27104	0.00807	10.90747	-0.11895	0.9984
PCN-250 (Fe_2Zn)	SO_2	-7388.70	1.83262	-0.00134	8.97E-07	-3.40E-10	17.70812	-0.00148	0.9913
	CO_2	-2904.16	0.73193	-0.00119	-1.02E-06	3.81E-09	8.86684	-0.00269	0.9989
	CH_4	-2540.06	7.67859	0.56857	-0.02737	5.02E-04	10.34157	-0.07308	0.9992
	N_2	-2461.25	0.49594	4.50835	-0.2705	0.00721	11.23868	-0.21779	0.9927

Table S5. Summary of the adsorption capacities of SO_2 with different partial pressures of SO_2, IAST selectivities of SO_2/CO_2, SO_2/CH_4, and SO_2/N_2 on various materials.

Materials	S_{BET} ($m^2\ g^{-1}$)	SO_2 uptake ($mmol\ g^{-1}$)		Selectivity for SO_2/CO_2 at 10/90 mixture	Selectivity for SO_2/CH_4 at 10/90 mixture	Selectivity for SO_2/N_2 at 10/90 mixture	Ref.
		0.1 bar	1.0 bar				
PCN-250 (Fe)	**1495**	**7.93**	**11.21**	**37**	**356**	**>1.0×10⁴**	
PCN-250 (Fe_2Co)	**1583**	**8.06**	**11.92**	**39**	**667**	**>1.0×10⁴**	
PCN-250 (Fe_2Ni)	**1619**	**8.64**	**12.45**	**27**	**208**	**>1.0×10⁴**	**This work**
PCN-250 (Fe_2Mn)	**1483**	**7.7**	**11.14**	**39**	**351**	**>1.0×10⁴**	
PCN-250 (Fe_2Zn)	**1560**	**8.21**	**12.11**	**50**	**339**	**>1.0×10⁴**	
Cu-ATC	600	6.9	8.0	114	750	>2.0×10⁶	4
HBU-20	1551	4.2	6.71	44.3	280	-	5
DMOF	1956	7.21	13.09	35	-	-	
DMOF-M	1557	6.4	12.15	38	-	-	6
DMOF-DM	1343	5.7	10.40	40	-	-	
DMOF-TM	900	6.43	9.68	169	-	-	
SIFSIX-1-Cu	1178	8.74	11.01	70.7	3145.7	1241.4	
SIFSIX-2-Cu-i	503	6.01	6.9	87.1	3103.2	1017.1	
SIFSIX-2-Cu	1881	-	6.5	-	-	-	7
SIFSIX-3-Zn	250	1.89	2.10	-	701.8	371.6	
SIFSIX-3-Ni	368	2.55	2.74	-	506.7	276.0	
ELM-12	706	1.95	2.73	30	871	4064	8
CPL-1	335	1	2	8.1			9
MOF-808-His	1054	5.20	10.36	90.5	-	-	10
MFM-601	3644	5.0	12.3	32	255	50	11
MFM-170	2408	6.50	17.5	35	-	-	12
MFM-300(Al)[b]		7.03 [b]	7.7 [b]				13
MFM-300(In)	1071	7.20	8.28	50	275	2700	14
MFM-300(Sc)	1360	7.79	9.4	30	-	-	15

	S_{BET}	SO_2 uptake (mmol g^{-1})		Selectivity for	Selectivity for	Selectivity for	
MFM-202a	2220	3.0	10.2	-	-	-	16
MFM-305	779	-	6.99	160	-	-	17
MFM-305-CH_3	256	-	5.16	145	-	-	
MFM-520	313	-	3.38	125[a]	-	20000[a]	18
NH_2-MIL-125(Ti)	1560	7.9[b]	10.8[b]	42[b]	-	-	
MIL-160	1170	5.5[b]	7.2[b]	124[b]	-	-	19
MOF-177		1 [b]	25 [b]				
Ni(bdc)$(ted)_{0.5}$	1783	4.54	9.97	-	-	-	20
ECUT-77	760	5.6	8.0	-	-	-	21
ECUT-100	688	3.3	4.95	-	-	-	22
ECUT-111	1493	6.4	11.56	25.2(1/99)	-	-	23
MIL-101(Cr)-4F	2176	4.6	18.4	-	-	-	24
Ni-gallate	455	3.79	4.49	25	$>1.0\times10^4$	$>1.0\times10^4$	
Co-gallate	494	4.51	5.28	143	$>1.0\times10^4$	$>1.0\times10^4$	25
Mg-gallate	576	5.19	5.81	321	$>1.0\times10^4$	$>1.0\times10^4$	
CAU-10	630	3.9	4.47		-	-	26
NU-200	1260	8.5	11.7	77	-	-	27
Fe-soc-MOF	1470	7.3	11.7	30	580	-	28
NKU-100	698	5	6.71	940[a]	-	>5000	29
CPL-1-NH_2	180	1.7	2.29	485	-	-	30
$Mn(INA)_2$	257	2.5	3.4	62.3	-	-	31
Zr-NU-907	1090	2.0	4.9	-	-	-	
Ce_5Zr-NU-907	730	2.2	4.6	-	-	-	32
Th-NU-907	610	3.4	5.7	-	-	-	
Zr-bptc	960	6.2	7.8	600[c]	-	>5 000 [c]	
MFM-422	3296	-	13.6	-	-	-	33
UiO-66-Cu^{II}	1068	3.0	8.2	54 [c]	-	-	
MFM-190(F)	2538	6.9	18.3	5.2 [c]	-	-	34

a. Volume ratio of SO_2:X mixture is 50:50; b. At a temperature of 293 K.; c. Volume ratio of SO_2:X mixture is 1:99

REFERENCES

1. D. Feng, K. Wang, Z. Wei, Y.-P. Chen, C. M. Simon, R. K. Arvapally, R. L. Martin, M. Bosch, T.-F. Liu, S. Fordham, D. Yuan, M. A. Omary, M. Haranczyk, B. Smit and H.-C. Zhou, *Nat. Commun.*, 2014, **5**, 5723.
2. Y. Chen, Z. Qiao, J. Huang, H. Wu, J. Xiao, Q. Xia, H. Xi, J. Hu, J. Zhou and Z. Li, *ACS Appl. Mater. Interfaces*, 2018, **10**, 38638-38647.
3. H. Wu, Y. Chen, Y. Yuan, D. Lv, S. Tu, Z. Liu, Z. Li and Q. Xia, *AIChE J.*, 2022, **68**, e17385.
4. Z. Zhu, K. Wu, X. Liu, P. Zhang, S. Chen, J. Chen, Q. Deng, Z. Zeng, S. Deng and J. Wang, *AIChE J.*, 2022, **68**, e17811.
5. Y.-B. Ren, H.-Y. Xu, S.-Q. Gang, Y.-J. Gao, X. Jing and J.-L. Du, *Chem. Eng. J.*, 2022, **431**, 134057.
6. S. Xing, J. Liang, P. Brandt, F. Schäfer, A. Nuhnen, T. Heinen, I. Boldog, J. Möllmer, M. Lange, O. Weingart and C. Janiak, *Angew. Chem., Int. Ed.*, 2021, **60**, 17998-18005.
7. X. Cui, Q. Yang, L. Yang, R. Krishna, Z. Zhang, Z. Bao, H. Wu, Q. Ren, W. Zhou, B. Chen and H. Xing, *Adv. Mater.*, 2017, **29**, 1606929.
8. Y. Zhang, Z. Chen, X. Liu, Z. Dong, P. Zhang, J. Wang, Q. Deng, Z. Zeng, S. Zhang and S. Deng, *Ind. Eng. Chem. Res.*, 2020, **59**, 874-882.
9. Y. Zhang, P. Zhang, W. Yu, J. Zhang, J. Huang, J. Wang, M. Xu, Q. Deng, Z. Zeng and S. Deng, *ACS Appl. Mater. Interfaces*, 2019, **11**, 10680-10688.
10. Z. Zhu, P. Zhang, B. Li, S. Chen, Q. Deng, Z. Zeng, J. Wang and S. Deng, *AIChE J.*, 2021, **67**, e17300.
11. J. H. Carter, X. Han, F. Y. Moreau, I. da Silva, A. Nevin, H. G. W. Godfrey, C. C. Tang, S. Yang and M. Schröder, *J. Am. Chem. Soc.*, 2018, **140**, 15564-15567.
12. G. L. Smith, J. E. Eyley, X. Han, X. Zhang, J. Li, N. M. Jacques, H. G. W. Godfrey, S. P. Argent, L. J. McCormick McPherson, S. J. Teat, Y. Cheng, M. D. Frogley, G. Cinque, S. J. Day, C. C. Tang, T. L. Easun, S. Rudić, A. J. Ramirez-Cuesta, S. Yang and M. Schröder, *Nat. Mater.*, 2019, **18**, 1358-1365.
13. S. Yang, J. Sun, A. J. Ramirez-Cuesta, S. K. Callear, W. I. F. David, D. P. Anderson, R. Newby, A. J. Blake, J. E. Parker, C. C. Tang and M. Schröder, *Nat. Chem.*, 2012, **4**, 887-894.
14. M. Savage, Y. Cheng, T. L. Easun, J. E. Eyley, S. P. Argent, M. R. Warren, W. Lewis, C. Murray, C. C. Tang, M. D. Frogley, G. Cinque, J. Sun, S. Rudić, R. T. Murden, M. J. Benham, A. N. Fitch, A. J. Blake, A. J. Ramirez-Cuesta, S. Yang and M. Schröder, *Adv. Mater.*, 2016, **28**, 8705-8711.
15. J. A. Zárate, E. Sánchez-González, D. R. Williams, E. González-Zamora, V. Martis, A. Martínez, J. Balmaseda, G. Maurin and I. A. Ibarra, *J. Mater. Chem. A*, 2019, **7**, 15580-15584.
16. S. Yang, L. Liu, J. Sun, K. M. Thomas, A. J. Davies, M. W. George, A. J. Blake, A. H. Hill, A. N. Fitch, C. C. Tang and M. Schröder, *J. Am. Chem. Soc.*, 2013, **135**, 4954-4957.
17. L. Li, I. da Silva, D. I. Kolokolov, X. Han, J. Li, G. Smith, Y. Cheng, L. L. Daemen, C. G. Morris, H. G. W. Godfrey, N. M. Jacques, X. Zhang, P. Manuel, M. D. Frogley, C. A. Murray, A. J. Ramirez-Cuesta, G. Cinque, C. C. Tang, A. G. Stepanov, S. Yang and M. Schroder, *Chem. Sci.*, 2019, **10**, 1472-1482.
18. J. Li, X. Han, X. Zhang, A. M. Sheveleva, Y. Cheng, F. Tuna, E. J. L. McInnes, L. J. McCormick McPherson, S. J. Teat, L. L. Daemen, A. J. Ramirez-Cuesta, M. Schröder and S. Yang, *Nat. Chem.*, 2019, **11**, 1085-1090.
19. P. Brandt, A. Nuhnen, M. Lange, J. Möllmer, O. Weingart and C. Janiak, *ACS Appl. Mater. Interfaces*,

2019, **11**, 17350-17358.
20. K. Tan, P. Canepa, Q. Gong, J. Liu, D. H. Johnson, A. Dyevoich, P. K. Thallapally, T. Thonhauser, J. Li and Y. J. Chabal, *Chem. Mater.*, 2013, **25**, 4653-4662.
21. Y. L. Fan, H. P. Zhang, M. J. Yin, R. Krishna, X. F. Feng, L. Wang, M. B. Luo and F. Luo, *Inorg. Chem.*, 2021, **60**, 4-8.
22. L. J. Guo, X. F. Feng, Z. Gao, R. Krishna and F. Luo, *Inorg. Chem.*, 2021, **60**, 1310-1314.
23. M. J. Yin, X. H. Xiong, X. F. Feng, W. Y. Xu, R. Krishna and F. Luo, *Inorg. Chem.*, 2021, **60**, 3447-3451.
24. E. Martínez-Ahumada, M. L. Díaz-Ramírez, H. A. Lara-García, D. R. Williams, V. Martis, V. Jancik, E. Lima and I. A. Ibarra, *J. Mater. Chem. A*, 2020, **8**, 11515-11520.
25. F. Chen, D. Lai, L. Guo, J. Wang, P. Zhang, K. Wu, Z. Zhang, Q. Yang, Y. Yang, B. Chen, Q. Ren and Z. Bao, *J. Am. Chem. Soc.*, 2021, **143**, 9040-9047.
26. J. A. Zárate, E. Domínguez-Ojeda, E. Sánchez-González, E. Martínez-Ahumada, V. B. López-Cervantes, D. R. Williams, V. Martis, I. A. Ibarra and J. Alejandre, *Dalton Transactions*, 2020, **49**, 9203-9207.
27. W. Gong, Y. Xie, T. D. Pham, S. Shetty, F. A. Son, K. B. Idrees, Z. Chen, H. Xie, Y. Liu, R. Q. Snurr, B. Chen, B. Alameddine, Y. Cui and O. K. Farha, *J. Am. Chem. Soc.*, 2022, **144**, 3737-3745.
28. Z. Chen, X. Wang, R. Cao, K. B. Idrees, X. Liu, M. C. Wasson and O. K. Farha, *ACS Mater. Lett.*, 2020, **2**, 1129-1134.
29. Z. Han, J. Li, W. Lu, K. Wang, Y. Chen, X. Zhang, L. Lin, X. Han, S. J. Teat, M. D. Frogley, S. Yang, W. Shi and P. Cheng, *Angew. Chem., Int. Ed.*, 2022, **61**, e202115585.
30. Z. Guo, Y. Li, P. Zhang, J. Cui, L. Chen, L. Yang, J. Wang, X. Cui and H. Xing, *Sep. Purif. Technol.*, 2022, **295**, 121337.
31. Z. Guo, J. Cui, Y. Li, P. Zhang, L. Yang, L. Chen, J. Wang, X. Cui and H. Xing, *Ind. Eng. Chem. Res.*, 2022, **61**, 5936-5941.
32. K. O. Kirlikovali, Z. Chen, X. Wang, M. R. Mian, S. Alayoglu, T. Islamoglu and O. K. Farha, *ACS Appl. Mater. Interfaces*, 2022, **14**, 3048-3056.
33. J. Li, G. L. Smith, Y. Chen, Y. Ma, M. Kippax-Jones, M. Fan, W. Lu, M. D. Frogley, G. Cinque, S. J. Day, S. P. Thompson, Y. Cheng, L. L. Daemen, A. J. Ramirez-Cuesta, M. Schröder and S. Yang, *Angew. Chem., Int. Ed.*, 2022, **61**, e202207259.
34. W. Li, J. Li, T. D. Duong, S. A. Sapchenko, X. Han, J. D. Humby, G. F. S. Whitehead, I. J. Victórica-Yrezábal, I. da Silva, P. Manuel, M. D. Frogley, G. Cinque, M. Schröder and S. Yang, *J. Am. Chem. Soc.*, 2022, **144**, 13196-13204.